Extensible Spherical Fibonacci Grids

Ricardo Marques, Christian Bouville, Kadi Bouatouch and Josep Blat

Abstract—Spherical Fibonacci grids (SFG) yield extremely uniform point set distributions on the sphere. This feature makes SFGs particularly well-suited to a wide range of computer graphics applications, from numerical integration, to vector quantization, among others. However, the application of SFGs to problems in which further refinement of an initial point set is required is currently not possible. This is because there is currently no solution to the problem of adding new points to an existing SFG while maintaining the point set properties. In this work, we fill this gap by proposing the extensible spherical Fibonacci grids (E-SFG). We start by carrying out a formal analysis of SFGs to identify the properties which make these point sets exhibit a nearly-optimal uniform spherical distribution. Then, we propose an algorithm (E-SFG) to extend the original point set while preserving these properties. Finally, we compare the E-SFG with a other extensible spherical point sets. Our results show that the E-SFG outperforms spherical point sets based on a low discrepancy sequence both in terms of spherical cap discrepancy and in terms of root mean squared error for evaluating the rendering integral.

Index Terms—Spherical Quasi-Monte Carlo, Low Discrepancy Spherical Point Sets, Adaptive Sampling, Rendering Equation

1 Introduction

Several works have shown the benefits of Fibonacci-based spherical distributions of points for various applications [2], [4], [10], [17], [19], [29]. The main strength of these point sets is an extremely uniform distribution which is near-optimal in terms of spherical cap discrepancy [5]. There are two families of such point sets: (i) spherical Fibonacci point sets based on planar Fibonacci *integration lattices* [24] (which, from here on, we will call spherical Fibonacci integration lattices, SFIL); (ii) and spherical Fibonacci point sets based on planar Fibonacci grids [28] (which, from here on, we will call spherical Fibonacci grids, SFG). SFILs constraint point set sizes to be Fibonacci numbers. An SFG, on the other hand, allows generating point sets with an arbitrary number of points. This freedom to choose the number of points justifies our interest in SFGs over SFILs.

In the particular case of computer graphics, SFGs have been successfully used for Quasi-Monte Carlo (QMC) spherical integration [19], vector quantization, texture filtering and procedural modeling [17], and, more recently, cone sampling for computation of the Shape Diameter Function [4]. In all these applications, the SFGs are shown to be more effective than alternative methods. However, despite their advantages, SFGs have an important limitation: they have a fixed size. Indeed there is currently no solution to the problem of adding more points to an existing spherical grid while keeping the characteristics of the SFG. This feature prevents the application of SFGs to *adaptive sampling schemes* in which the sampling rate might be increased on the fly according to some quality criterion to refine the QMC estimate. In fact, a direct application of SFGs to an adaptive sampling scheme would imply discarding all previous samples when increasing the sampling rate, which is unpractical when the cost of obtaining a sample is extremely high as, for example, in photo-realistic rendering. In this article we fill this gap by proposing a method for generating *extensible spherical Fibonacci grids (E-SFG)*, which allows adding new points to the original point set in a sequential manner. Moreover, we show that the resulting point set maintains the uniformity properties of the original point set. Our work brings three main contributions which we list below:

1) A thorough analysis of SFGs where we provide a new set of formal proofs demonstrating the SFG point set properties.
2) An algorithm for producing extensible spherical Fibonacci grids (E-SFG) which leverages the properties previously demonstrated. We prove that the resulting E-SFGs preserve the properties of the SFG point sets.
3) An analysis of the efficiency of the resulting E-SFG point set for computer graphics applications, both through theoretical metrics, as well as through a set of numerical experiments.

This article is structured as follows: in the next section we review the related work. In Sec. 3, we provide a set of interesting properties of SFGs which have been stated in previous works. Our contribution starts in Sec. 4 where we perform an in-depth analysis of SFGs and derive new properties. These properties are then used in Sec. 5 for the E-SFG point set construction and to verify that the extended point set maintains the good properties of the original SFG. Finally, we present and discuss our results in Secs. 6 and 7, respectively, followed by the conclusions in Sec. 8.

2 Related Work

Our goal in this paper is to address the specific problem of extensibility for spherical Fibonacci grids and not the much more general problem of sampling on the sphere which has been extensively covered in the literature. For a detailed analysis of point systems on the sphere, refer to [15] which is, to our knowledge, the latest review on this topic.

- *R. Marques and J. Blat are with Universitat Pompeu Fabra, Grup de Recerca de Tecnologies Interactives, Barcelona, Spain. E-mail: ricardo.marques@upf.edu*
- *C. Bouville and K. Bouatouch are with IRISA, University of Rennes 1, Rennes, France.*

Manuscript received MONTH DAY, 2018; revised MONTH DAY, YEAR.

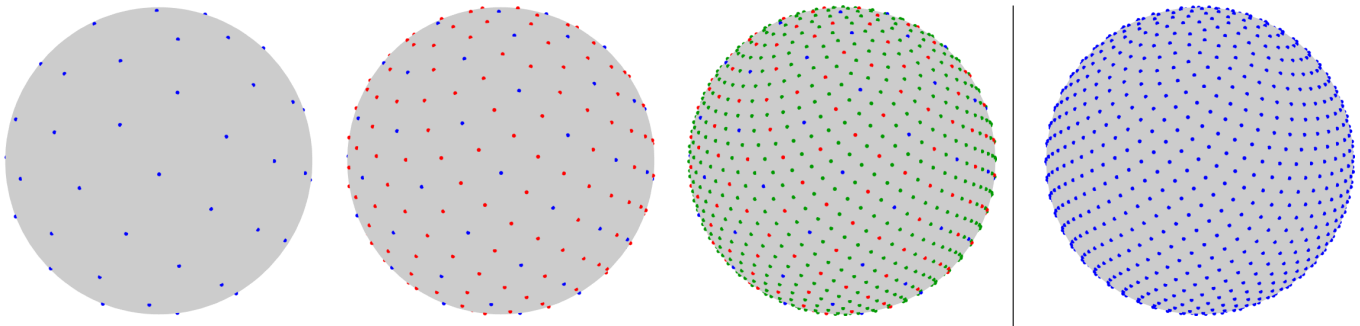

(a) Initial spherical grid with 64 points (b) Extension to 256 points (c) Extension to 1024 points (d) Classic spherical Fibonacci grid with 1024 points

Fig. 1. Example of our extensible spherical Fibonacci grid (E-SFG). The initial spherical grid in (a) contains 64 points shown in blue. In (b) the initial grid is extended to 256 points, by adding 192 new points (marked in red). The resulting point set is further extended in (c), yielding a total of 1024 points. Finally, (d) shows an example of a classical (not extensible) spherical Fibonacci grid (SFG). The figures show that our E-SFG algorithm can generate extensible spherical point sets with a distribution visually similar to those of classical SFG. Quantitative results shown later in the paper confirm this observation. They show that our approach yields extensible point sets with similar properties in terms of spherical discrepancy and root mean square integration error, overcoming the fixed-size constraint of classic spherical Fibonacci grids without impairing their properties.

We start by briefly defining key concepts for understanding the remainder of this work. An *integration lattice* for functions over $\mathbb{R}^2$ is a lattice containing $\mathbb{Z}^2$ as a subset [8], [24]. Let us now call P_N the subset of points of a lattice L contained in $[0,1)^2$ and projected onto the surface of the unit sphere. If L is an integration lattice then P_N is said to form a spherical integration lattice. If L is not an integration lattice, then P_N forms a spherical grid.

Spherical Fibonacci integration lattices (SFIL), used for numerical integration on the sphere, were first introduced by Hannay and Nye [14]. In their paper the authors show that, by projecting a unit square Fibonacci integration lattice (as defined by Niederreiter and Sloan [21]) onto a sphere through a Lambert cylindrical equal-area transform, particularly efficient point sets for numerical integration over the sphere can be found. Furthermore, they highlight the topological properties that make the SFIL so efficient for numerical integration on the sphere. These good properties for numerical integration have been analyzed in details by Aistleitner et al. [1]. Swinbank and Purser [28] further improve the point set properties by shifting the z-coordinate of the projected points so as to obtain a better distribution at the poles. Additionaly, they introduce the spherical Fibonacci grids (SFG), a point set whose size is not restricted to Fibonacci numbers as opposed to SFIL. Swinbank and Purser also derive interesting properties of the SFG which we use in this paper. González [12] applies SFGs to the measurement of areas on a sphere. SFGs are also appropriate for numerical integration of the shading integral as shown by Marques et al. [19]. They show that SFGs outperform all familiar QMC point sets for diffuse and glossy reflections when evaluating shading integrals.

However, compared with standard Monte Carlo importance sampling methods such as [3] or digital net sequences, such as Halton or Sobol sequences, SFGs have the disadvantage of not being extensible. This means that if the integration error is deemed too significant, requiring a larger point set, none of the points of the previous point set will be included in the new larger point set, thus wasting all previously-drawn samples. To solve this problem in the case of planar integration lattices, Hickernell et al. [16] introduce the concept of *extensible integration lattice sequences*. They are able to extend unit square rank-1 integration lattices [8] (i.e., integration lattices which can be obtained by the rule $p_k = \frac{k}{N}\mathbf{v} \bmod (1)$, where $\mathbf{v}$ is the generating vector with coordinates in $\mathbb{N}$ and N the point set size), hence generating infinite sequences of points similar to digital net sequences. A similar approach has been applied in [9] to anti-aliasing and texture representation. In [18], the author proposes a shifted replication method in order to extend a rank-1 integration lattice for generating stratified samples set. However, all these methods cannot be applied to our problem since SFGs projected onto the unit square are not integration lattices as we explain in this paper. Cools and Nuyens [7] analyze the specific case of extensions of Fibonacci integration lattices but again, their solution does not apply to SFGs for the same reason as above. Furthermore, when lifted onto the sphere, the extended point sets no longer exhibit the nice topological properties of the original SFIL. Our goal in this paper is thus to propose a solution for extending SFGs which preserves the properties that make the SFG point set efficient for spherical integration. An example of the resulting point set, named E-SFG (extended spherical Fibonacci grid), is shown in Fig. 1.

3 Background

Spherical Fibonacci grids and some of their properties have been studied in previous works. In this section, we state the most relevant properties for our goal. Some of them, such as the basis vectors of an SFG, have not been formally demonstrated in the related work. In this case, we state these properties in this section and provide a formal derivation as part of our contribution in the following sections.

SFGs are directly defined on the *unit sphere*. Given the desired number of points N, the spherical coordinates (θ, ϕ) of the j^{th} point of the SFG are given by [19], [28]:

$$\left.\begin{aligned} \theta_j &= \arccos(1 - 2j/N) \\ \phi_j &= 2j\pi\Phi^{-1} \bmod 2\pi \end{aligned}\right\} \quad 0 \leq j < N \qquad (1)$$

where θ_j is the elevation angle, ϕ_j is the azimuth angle, and $\Phi = (1+\sqrt{5})/2$ is the golden ratio. An example of

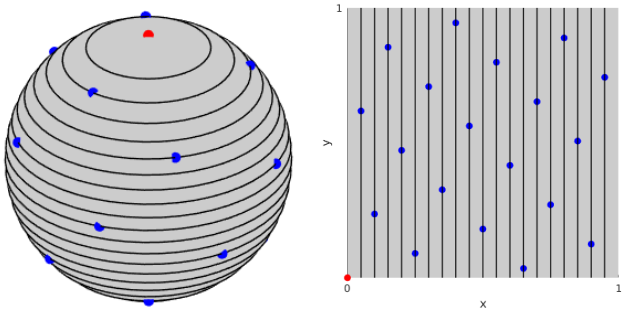

(a) Spherical Fibonacci grid (SFG) (b) Planar Fibonacci grid (F_G)

Fig. 2. (a) Example of a spherical Fibonacci grid (SFG) with 20 points, as defined in Eq. (1). (b) Planar Fibonacci grid (F_G, Eq. (3)) resulting from projecting (a) to the unit square through Eq. (2).

the resulting point set for $N = 20$ is given in Fig. 2 (a). In an SFG, all points are evenly distributed along the vertical axis $z = \cos\theta$. The difference between the z components of two successive points is constant: $z_j - z_{j+1} = 2/N$ (c.f. Eq (1)). This guarantees that there is a single point within each zone defined by the two parallels at z_j and z_{j+1}, as shown in Fig. 2 (a). Similarly, the difference between the azimuth angles of two successive points has a constant value $2\pi\Phi^{-1}$. Such an angular spacing leverages the fact that the golden ratio is the most irrational number, hence avoiding periodicities in the ϕ angle distribution while providing a regular distribution. Finally, note that the SFG of Eq. (1) (and Fig. 2 (a)) is sometimes expressed with a shift of $1/2N$ in the z-axis [19], [28]. This shift symmetrizes the z-coordinate distribution so that the first and last points are at equal distances from their closest pole, which improves the spherical discrepancy of the point set (more details on this metrics are given below). For the sake of simplicity, and without loss of generality, this shift is ignored in this section but it is reintroduced in Sec. 5 for the specific case of E-SFG.

In order to make a detailed analysis of the SFG, it is convenient to project it onto the unit square through the Lambert cylindrical equal area projection [28]:

$$\begin{aligned} x &= (1 - \cos\theta)/2 \\ y &= \phi\,(2\pi)^{-1}\,. \end{aligned} \tag{2}$$

In this case, the point set resulting from the application of Eq. (2) to the SFG point set defined by Eq. (1) generates a planar Fibonacci grid (F_G). The Cartesian coordinates (x_j, y_j) of the j^{th} point of a planar F_G are given by:

$$\left.\begin{aligned} x_j &= j/N \\ y_j &= \text{frac}\left(\tfrac{j}{\Phi}\right) \end{aligned}\right\} \quad 0 \le j \le N \tag{3}$$

An example of such a planar Fibonacci grid F_G is shown in Fig. 2(b). To each of the zones shown on the sphere in Fig. 2(a) corresponds a vertical equal-area slice on the unit square in Fig. 2(b), with each zone (and slice) containing a single point.

A planar Fibonacci grid F_G can be alternatively defined as the subset $F_G = F_L \cap [0,1[^2$ of a planar Fibonacci *lattice* F_L defined by:

$$F_L = \left\{\mathbf{p} = z_0\,\mathbf{b}_k + z_1\,\mathbf{b}_{k+1} \;:\; (z_0, z_1) \in \mathbb{Z}^2\right\}\,. \tag{4}$$

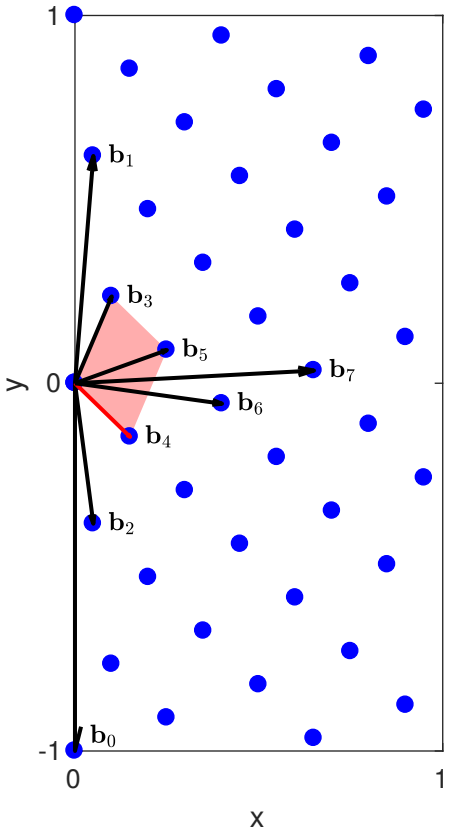

Fig. 3. Basis vectors of a planar Fibonacci lattice F_L generated with $N = 20$. Only the lattice points within the $[0,1] \times [-1,1]$ rectangle are shown. The pink area denotes the area of the unit cell formed by the basis vectors $\mathbf{b}_3$ and $\mathbf{b}_4$. The red vector (b_4) indicates the shortest basis vector.

Each point $\mathbf{p}$ in F_L can be expressed as an integer combination of the basis vectors $\mathbf{b}_k$ and $\mathbf{b}_{k+1}$ defined below. Note that the points in F_L are no longer restricted to the unit square as opposed to those belonging to a planar Fibonacci grid F_G. As we show below, the notion of planar Fibonacci lattice F_L, as defined by Eq. (4), is particularly interesting, since its formulation allows deriving certain properties of the point set which can then be transposed to the SFG. Based on this representation, Swinbank and Purser [28] observe that the basis vectors of a planar Fibonacci lattice F_L are the pairs $(\mathbf{b}_k, \mathbf{b}_{k+1})$ with:

$$\mathbf{b}_k = \left(\frac{F_k}{N}, \frac{(-1)^{k-1}}{\Phi^k}\right), \quad k = 0, 1, \ldots, k_m\,, \tag{5}$$

and k_m such that:

$$F_{k_m} \le N < F_{k_m+1}\,,$$

N being the number of points on the grid, and F_{k_m} being the largest Fibonacci number smaller or equal to N. However, in their paper, Swinbank and Purser give no mathematical proof of this observation. In subsubsection 4.3, we provide a formal derivation of the basis vectors of the planar Fibonacci lattice F_L. Fig. 3 shows the set of basis vectors for a planar Fibonacci lattice F_L with $N = 20$ points. In this case, and according to Eq. (5), the number of basis vectors is $k_m +$

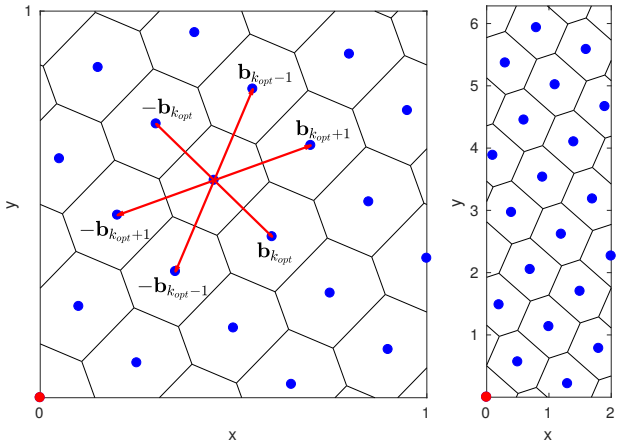

(a) Original lattice (b) Stretched lattice

(c) After projection onto the unit sphere

Fig. 4. (a) Voronoi cells of a planar Fibonacci lattice F_L. (b) Voronoi cells of the same lattice scaled to the $[0, 2] \times [0, 2\pi]$ rectangle. Observe that the Voronoi cells are not elongated after stretching. (c) Voronoi diagram of a SFG.

$1 = 8$. The basis vectors $\mathbf{b}_k$ satisfy a recurrence relationship similar to that of Fibonacci numbers:

$$\mathbf{b}_{k+1} = \mathbf{b}_k + \mathbf{b}_{k-1} \ , \tag{6}$$

as pointed out by Swinbank and Purser [28]. As explained below, these vectors will be our basic tool for extending the spherical Fibonacci grid. Associated with any lattice basis given by $(\mathbf{b}_k, \mathbf{b}_{k+1})$ is the notion of *unit cell*. A unit cell, or fundamental paralelogram, is the area associated with any pair of vectors forming a basis of the lattice [23]. It can be seen as the smallest group of lattice points which constitute a repeating pattern in the lattice. In general, the unit cell is illustrated using a pair of short, nearly orthogonal basis vectors as shown in Fig. 3. However, since the basis is not unique, there is not a single unit cell in the Fibonacci lattice, and we can use any pair of basis vectors $(\mathbf{b}_k, \mathbf{b}_{k+1})$ to form unit cells of the Fibonacci lattice. Note that, by definition, the unit cell does not contain any point in its interior.

Another relevant property of planar Fibonacci grids F_G is illustrated in Fig. 4. As observed by Hannay and Nye [14], the shape of the Voronoi cells of a planar Fibonacci grid F_G (as defined in Sec. 4.5) is not modified when the grid is streched with different scaling factors along the x and y

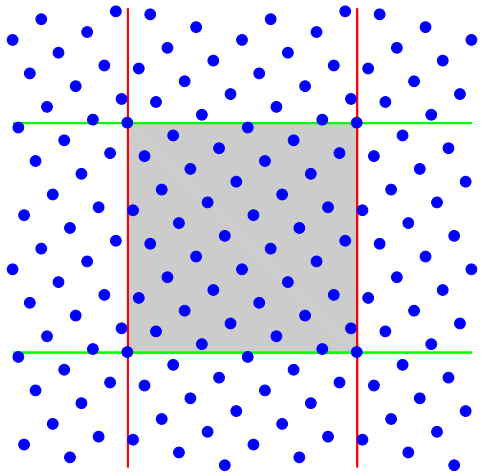

Fig. 5. Periodicity properties of a planar Fibonacci grid F_G. This figure has been obtained by shifting the (unit square) planar Fibonacci grid, shown over a gray background. The periodicity along the green edges, and the non-periodicity along the red edges becomes evident.

axis, although the cells orientation and size change. More specifically, the Voronoi cells are not elongated as opposed, for example, to the case of regular axes-aligned square unit cell lattice [14]. This remarkable property explains why the uniformity of planar Fibonacci grid is well preserved when lifted to the sphere, despite the non-uniform scale factor introduced by the Lambert cylindrical projection. In Sec. 4.5, we provide a mathematical proof of this invariance property which, as shown below, is also preserved by our proposed E-SFG (extended SFG) algorithm.

Finally, as shown in Sec. 4.3 and illustrated in Fig. 5, the planar Fibonacci lattice F_L is not periodic in the x-direction, which means that F_L does not contain $\mathbb{Z}^2$ as a subset. The non-periodicity in the x-direction prevents the application of point set extension techniques developed for integration lattices (i.e., fully periodic unit hypercube grids) such as those proposed by Hickernell et al. [16] and by Cools and Nuyens [7]. Moreover, these approaches do not target the unit sphere, and thus do not maintain the beneficial non-elongation property of the Voronoi cell.

Summary and overview: The properties mentioned above make the spherical Fibonacci grid (SFG) particularly well-suited to applications relying on a high quality uniform distribution of points on the sphere. However, a broader use of SFGs is currently hindered by the absence of extensibility as explained in Sec. 1. We fill this gap by proposing an efficient algorithm for extensible spherical Fibonacci grids (E-SFG). Our contribution starts in the following section (Sec. 4) with an in-depth formal analysis of SFG properties. With this analysis, we identify the characteristics of the planar Fibonacci grids which enable us to preserve their uniformity properties when projected onto the sphere. Then, in Sec. 5, we propose our E-SFG algorithm. The point set extension is performed in the projected unit square domain, and is designed to maintain the properties identified in Sec. 4. Therefore, when the resulting point set is projected back onto the unit sphere, the uniformity of the original distribution is preserved.

4 GEOMETRY OF SPHERICAL FIBONACCI GRIDS

4.1 Useful identities

The mathematical developments presented in this section use the following equations related to the golden ratio Φ and Fibonacci numbers F_k (see e.g. [13]):

$$1 = \Phi - \Phi^{-1} \tag{7}$$

$$\sqrt{5} = \Phi + \Phi^{-1} \tag{8}$$

$$F_k = \frac{\Phi^k - (-\Phi)^{-k}}{\sqrt{5}} \tag{9}$$

From Eq. (8) and (9), it is easy to derive the following equation:

$$F_k \Phi^{-1} = F_{k-1} - (-\Phi)^{-k}\,. \tag{10}$$

Another useful identity is [13]:

$$F_{4m} = F_{2m}\left(F_{2m+1} + F_{2m-1}\right)\,, \tag{11}$$

from which we can show using Eq. (9):

$$\Phi^{2m} + \Phi^{-2m} = F_{2m+1} + F_{2m-1}\,. \tag{12}$$

4.2 Unit cell area of an SFG

Suitable lattices for QMC numerical integration must have unit cell area of $1/N$. In the case of integration lattices, the unit cell has always an area of $1/N$ [20], [24]. However, as mentioned above, the SFG is not an integration lattice and thus this property is yet to be proven in the SFG case. In the following we prove that SFGs also have a unit cell area of $1/N$.

The proof we propose is performed in two steps. First, we show that the unit cell area of a planar Fibonacci lattice F_L (i.e., the area of the parallelogram spanned by a given pair of basis vectors $(\mathbf{b}_k, \mathbf{b}_{k+1})$) is $1/N$ whatever the considered pair of basis vectors $(\mathbf{b}_k, \mathbf{b}_{k+1})$. Then, we explain how this proof can be transposed to an SFG (i.e., to the unit sphere, our space of interest).

Let us consider the general equation of the planar Fibonacci lattice F_L as given by Eq. (4). Assuming that the basis vectors are provided by Eq. (5), Eq. (4) can be rewritten in matrix form as:

$$F_L = \left\{ \mathbf{p} = (x, y) \;:\; \begin{bmatrix} x \\ y \end{bmatrix} = \mathbf{M} \begin{bmatrix} z_0 \\ z_1 \end{bmatrix},\ (z_0, z_1) \in \mathbb{Z}^2 \right\} \tag{13}$$

with:

$$\mathbf{M} = \begin{bmatrix} \dfrac{F_k}{N} & \dfrac{F_{k+1}}{N} \\ \dfrac{(-1)^{k-1}}{\Phi^k} & \dfrac{(-1)^k}{\Phi^{(k+1)}} \end{bmatrix}. \tag{14}$$

M is thus a matrix where each column represents a basis vector, i.e., $\mathbf{b}_k$ and $\mathbf{b}_{k+1}$, respectively. Following the terminology of lattice theory, let us call a *unit cell* the area enclosed by two basis vectors. Then the area of the unit cell defined by the parallelogram spanned by any basis vector pair $(\mathbf{b}_k, \mathbf{b}_{k+1})$ can be simply retrieved by computing the determinant Δ_M of the matrix M, yielding:

$$\Delta_M = \frac{F_k}{N}\frac{(-1)^k}{\Phi^{(k+1)}} - \frac{F_{k+1}}{N}\frac{(-1)^{k-1}}{\Phi^k} = (-1)^k \frac{1}{N} \tag{15}$$

by application of Eqs. (8) and (9).

The result presented in Eq. (15) is obtained for planar Fibonacci lattices F_L (Eq. (4)), i.e., a planar Fibonacci lattice not restricted to the unit square. However, the unit cell generated by the basis vectors $\mathbf{b}_0, \mathbf{b}_1$ is of a special interest. Indeed, this is the sole basis vector pair generating unit cells that do not exceed the unit square boundaries in the non-periodic direction of the planar Fibonacci grid F_G (i.e., the x direction). This periodicity property makes planar Fibonacci grids apt for numerical integration of functions $f(x, y)$ in $\mathbb{R}^2$ that are periodic for the y variable only. Finally, extending the proof to SFGs is straightforward since the spherical projection considered (Eq. (2)) is equal area, and thus the area corresponding to each grid point remains equal.

4.3 Formal proof of the basis vectors of an SFG

We want to demonstrate that any pair of vectors $(\mathbf{b}_k, \mathbf{b}_{k+1})$ given by Eq. (5) are basis vectors of the planar Fibonacci lattice F_L defined by Eq. (4). We show in the following that any point in F_L can be expressed through an integer linear combination of $(\mathbf{b}_k, \mathbf{b}_{k+1})$. Formally, this can be proved by inverting Eq. (13) such that:

$$\begin{bmatrix} z_0 \\ z_1 \end{bmatrix} = \mathbf{M}^{-1} \begin{bmatrix} x \\ y \end{bmatrix} \tag{16}$$

and showing that z_0 and z_1 are integers for every point (x, y) in the planar Fibonacci grid. Using Eq. (14) and Eq. (15), we have:

$$\mathbf{M}^{-1} = (-1)^k N \begin{bmatrix} -(-\Phi)^{-k-1} & -\dfrac{F_{k+1}}{N} \\ (-\Phi)^{-k} & \dfrac{F_k}{N} \end{bmatrix}. \tag{17}$$

Then, using the (x, y) coordinates of the j^{th} Fibonacci grid point as expressed by Eq. (3), we obtain for the z_0 coordinate:

$$z_0 = (-1)^k \left[-j(-\Phi)^{-k-1} - F_{k+1} \operatorname{frac}\left(\frac{j}{\phi}\right) \right]. \tag{18}$$

Using Eq. (10), Eq. (18) can be transformed as follows:

$$z_0 = (-1)^k \left[-jF_k + F_{k+1}\left(\frac{j}{\Phi} - \operatorname{frac}\left(\frac{j}{\Phi}\right)\right) \right] \tag{19}$$

$$= (-1)^k \left[-jF_k + F_{k+1} \operatorname{floor}\left(\frac{j}{\Phi}\right) \right], \tag{20}$$

which shows that the z_0 coordinate value is an integer for all points of the Fibonacci grid. Proceeding similarly for the z_1 coordinate, we get:

$$z_1 = (-1)^k \left[jF_{k-1} - F_k \operatorname{floor}\left(\frac{j}{\Phi}\right) \right], \tag{21}$$

which is also an integer value, which proves that the pair of vectors $(\mathbf{b}_k, \mathbf{b}_{k+1})$ are basis vectors of the lattice. The recurrence Eq. (6) is easily derived from the basic recurrence equation of Fibonacci numbers and Eq. (7).

Eq. (16) can also be used to make a compact proof of the periodicity in the y-direction (and the non-periodicity in the x-direction) of a planar Fibonacci grid F_G. Let us consider a point $\mathbf{p}_j = [x_j, y_j]^t$ of the planar Fibonacci *grid* F_G (cf. Eq. (3)), and a vector $\mathbf{v}_m = [0, m]^t$ with $m \in \mathbb{Z}$. Our goal is to show that $\mathbf{p} + \mathbf{v}_m \in F_L$, with F_L being

the full planar Fibonacci *lattice* as defined by Eq. (4). Using Eq. (16), the translation of point $\mathbf{p}$ by $\mathbf{v}_m$ results in adding $[-mF_{k+1}, mF_k]^t$ to the $[z_o, z_1]$ coordinates with respect to the $(\mathbf{b}_k, \mathbf{b}_{k+1})$ basis vectors. As the coordinates of this translation vector are in $\mathbb{Z}$, the translated point is also a point of the lattice F_L, hence the periodicity. It can be easily verified that this condition is not satisfied for a translation in the x direction. This is due to the fact that the first column of $\mathbf{M}^{-1}$ has irrational coefficients whereas the last column has coefficients in $\mathbb{Z}$.

4.4 Minimum distance between points

The uniformity of a point set distribution is directly related to the minimum distance between the points [15], [19]. Intuitively, one can see that the larger the minimum distance between points, the more uniform the distribution. Therefore, having an analytic expression for the minimum distance is a valuable tool to assess the quality of the point set. As shown by Brauchart and Dick [5], such properties are well-preserved when lifting a point set from the plane to the sphere using an equal area transform, except near the poles. Therefore, to facilitate obtaining analytical results, in the following we show how to derive such an expression for the planar Fibonacci grid. Moreover, as explained in Sec. 5, this expression allows us to show that the minimum distance property is preserved with our point set extension algorithm, E-SFG.

Let us thus express the square of the length of the basis vector $\mathbf{b}_k$ as follows:

$$l^2(k) = \frac{F_k^2}{N^2} + \Phi^{-2k}\,. \tag{22}$$

Then, solving for k satisfying the equation $\frac{dl^2}{dk} = 0$, yields the index k_{opt} of the smallest basis vector, given by:

$$k_{opt} = \mathrm{nint}\left(\frac{\ln(5N^2+1)}{4\ln(\Phi)}\right), \tag{23}$$

where $\mathrm{nint}()$ denotes the nearest integer function. For the interested reader, a detailed derivation of Eq. (23) is given in subsubsection 4.4.1.

A fundamental property of a lattice unit cell is that it does not contain any point of the lattice in its interior [6]. As $\mathbf{b}_{k_{opt}}$ is the shortest basis vector, the vectors $\mathbf{b}_{k_{opt}}$, $\mathbf{b}_{k_{opt}+1}$ and $\mathbf{b}_{k_{opt}-1}$ necessarily give the nearest neighbors of any lattice point as shown in Fig. 4(a). This is because the unit cells defined by $(\mathbf{b}_{k_{opt}}, \mathbf{b}_{k_{opt}+1})$ and $(\mathbf{b}_{k_{opt}}, \mathbf{b}_{k_{opt}-1})$ cannot contain any other point of the lattice. Moreover, from the recursion property $\mathbf{b}_{k+1} = \mathbf{b}_k + \mathbf{b}_{k-1}$ (Eq. (6)), it follows that any triangle formed with two successive basis vectors $\mathbf{b}_k$ and $\mathbf{b}_{k+1}$ has $\mathbf{b}_{k-1}$ as third edge. If $\mathbf{b}_k$ has been selected as the shortest basis vector, all edges of the triangle formed with $\mathbf{b}_k$ and $\mathbf{b}_{k+1}$ are necessarily longer than $\mathbf{b}_k$. Please refer to the supplemental material for further details on the relationship between nearest neighbors and the shortest basis vectors.

The minimum distance between points in a planar Fibonacci grid F_G of size N is thus given by $d_{min} = l(k_{opt})$. As shown in subsubsection 4.4.2, d_{min} can be bounded by:

$$\sqrt{\frac{2}{\sqrt{5}}}\frac{1}{\sqrt{N}} < d_{min} < \frac{1}{\sqrt{N}}\,, \tag{24}$$

where the constant $\sqrt{\frac{2}{\sqrt{5}}} \approx 0.946$. Eq. (24) shows that the minimum distance d_{min} between points on a planar Fibonacci grid F_G is in $O(N^{-1/2})$, and provides a good characterization of the uniformity of the point distribution for planar Fibonacci grids. Moreover, Eq. (24) is also used in the remainder of this article to show that our proposed E-SFG generator provides point sets which have the same d_{min} property.

4.4.1 Deriving k_{opt}

The square of the length of the basis vector $\mathbf{b}_k$ is:

$$l^2(k) = \frac{F_k^2}{N^2} + \Phi^{-2k} \tag{25}$$

which can be rewritten as follows using Eq. (9):

$$l^2(k) = \frac{\left(\Phi^k - (-\Phi)^{-k}\right)^2}{5N^2} + \Phi^{-2k} \tag{26}$$

As $dl^2/dk = 2l\,dl/dk$ and $l \neq 0$, dl^2/dk and dl/dk are zero for the same value of k, so the minimum vector length is reached when $dl^2/dk = 0$, that is:

$$\frac{dl^2}{dk} = 2\ln(\Phi)\left(\frac{\Phi^{2k} - \Phi^{-2k}}{5N^2} - \Phi^{-2k}\right) = 0\,. \tag{27}$$

Finally, solving the above equation, and noting that $l^2(k)$ is convex and symmetric with respect to the minimum (as shown in the supplemental material), yields:

$$k_{opt} = \mathrm{nint}\left(\frac{\ln(5N^2+1)}{4\ln(\Phi)}\right)$$

as stated in Eq. (23), where 'nint' denotes the nearest integer function. Note that, from the convexity and symmetry of $l^2(k)$, we can also infer that $\mathbf{b}_{k_{opt}}$, $\mathbf{b}_{k_{opt}+1}$ and $\mathbf{b}_{k_{opt}-1}$ are the three shortest basis vectors. This property will be used in Sec. 4.5.

4.4.2 Bounding the length of k_{opt}

In practice, $5N^2 \gg 1$ so we can use the following approximation:

$$k_{opt} \approx \tilde{k}_{opt} = \mathrm{nint}(r)\,, \quad \text{with} \quad r = \left(\frac{\ln(N\sqrt{5})}{2\ln(\Phi)}\right), \tag{28}$$

and proceeding similarly for $l^2(k)$, we have from Eq. (26):

$$l^2(k) \approx \tilde{l}^2(k) = \frac{\Phi^{2k}}{5N^2} + \Phi^{-2k}. \tag{29}$$

These approximations are perfectly acceptable given the point set sizes currently used in applications (please refer to the supplemental material for more details). Moreover, we can drop the nint() function in Eq. (28), yielding:

$$\tilde{k}_{opt} = r + \alpha \;\text{ with }\; -0.5 \leq \alpha \leq 0.5, \tag{30}$$

The minimum for $d_{min} \approx \tilde{l}(\tilde{k}_{opt})$ is reached when r is close to an integer (i.e., $\alpha = 0$). In this case, and recalling that $e^{\ln(y)} = y$, we have from Eqs. (29) and (30):

$$d_{min}^{-} \approx \tilde{l}(r) = \sqrt{\frac{2}{\sqrt{5}}}\frac{1}{\sqrt{N}}, \tag{31}$$

and the maximum when r is as far as possible from an integer (i.e., $\alpha = \pm 0.5$), that is:

$$d^{+}_{min} \approx \tilde{l}(r \pm 0.5) = \frac{1}{\sqrt{N}} \tag{32}$$

and thus we have:

$$\sqrt{\frac{2}{\sqrt{5}}}\frac{1}{\sqrt{N}} < d_{min} < \frac{1}{\sqrt{N}}, \tag{33}$$

which proves Eq. (24).

4.5 The Voronoi cell shape

We start our analysis with the commonly-accepted observation that the Voronoi cells in a planar Fibonacci lattice are always hexagonal and that their shape is determined by the six nearest neighbors of any point $\mathbf{p}$ of the lattice. As mentioned in Sec. 3, the Voronoi cells of planar Fibonacci grids are not elongated under grid stretching (see Fig. 4). This feature results from the layout of the three particular basis vectors $\mathbf{b}_{k_{opt}-1}$, $\mathbf{b}_{k_{opt}}$, $\mathbf{b}_{k_{opt}+1}$, which are the shortest among the $\{\mathbf{b}_k\}$ set (as shown before in Sec. 4.4.1). Thanks to the pointwise symmetry property of lattices, $\pm\mathbf{b}_{k_{opt}-1}$, $\pm\mathbf{b}_{k_{opt}}$ and $\pm\mathbf{b}_{k_{opt}+1}$ determine the location of the six neighboring points (see Fig. 4(a)), and thus the shape of the typical six-sided Voronoi cell of a planar Fibonacci grid. The shape of Voronoi cells can be characterized by the elongation parameter $r_s = \|\mathbf{b}_l\|/\|\mathbf{b}_s\|$, which is the ratio between the longest and the shortest basis vectors among $\mathbf{b}_{k_{opt}-1}$, $\mathbf{b}_{k_{opt}}$ and $\mathbf{b}_{k_{opt}+1}$. Note that r_s does not aim at fully defining the Voronoi cell shape, but instead it is used to capture the uniformity of the point set distribution: if the cell is elongated in one direction, then this indicates anisotropy in the Voronoi cell shape which implies a less uniform point set distribution. As we show in subsubsection 4.5.1, the elongation parameter r_s of a planar Fibonacci grid F_G is bounded by $\sqrt{3/2} < r_s < \sqrt{2}$, which denotes a quite compact Voronoi cell shape. Moreover, we demonstrate in subsubsection 4.5.2 that when the planar Fibonacci grid is streched by some factors s_x and s_y (in the x- and y-coordinates, respectively), the resulting elongation factor r'_s of the new Voronoi cells lies within the same bounds as for the original Fibonacci grid (i.e., $\sqrt{3}/2 < r'_s < \sqrt{2}$). This particularly interesting result explains why the shape of Voronoi cells of a planar Fibonacci grid is practically invariant under grid scaling.

As the mapping of the planar Fibonacci grid F_G to the sphere can be locally approximated by a stretching transformation (i.e., a scaling by s_x and s_y) except near the poles, this explains why the Voronoi cells of an SFG as shown in Fig. 4(c) still exhibit a relatively regular shape after the spherical projection. This also motivates the interest in the analysis of the planar F_G when considering the projection onto the sphere. Note however that, due to the distortion introduced by the mapping from the plane to the sphere, this approximation does not hold near the poles because of the particular topology of the Voronoi cells in these regions, but this concerns a very small proportion of Voronoi cells (cf. Keinert et al. [17] and Swinbank and Purser [28]). As the Voronoi cells invariance property is fundamental to explain the uniformity of an SFG, it is thus very important that our proposed extension method preserves this particular basis vector layout.

4.5.1 The bounds of r_s

We want to prove that the ratio r_s between the largest and the smallest basis vectors among $b_{k_{opt}-1}, b_{k_{opt}}$ and $b_{k_{opt}+1}$ is bounded by $\sqrt{3/2} < r_s < \sqrt{2}$. Plugging Eq. (30) into Eq. (29) yields the length of the smallest of the three vectors, $b_{k_{opt}}$:

$$\tilde{l}^2(\tilde{k}_{opt}) = \frac{1}{N\sqrt{5}} f(\alpha)\,, \quad -0.5 \le \alpha \le 0.5\,, \tag{34}$$

with

$$f(\alpha) = \Phi^{2\alpha} + \Phi^{-2\alpha}\,, \tag{35}$$

which proves that $\tilde{l}^2(\tilde{k}_{opt})$ is convex and symmetric about its minimum. Proceeding similarly for the basis vectors with index $k_{opt} - 1$ and $k_{opt} + 1$, we get:

$$\tilde{l}^2(\tilde{k}_{opt} + m) = \frac{1}{N\sqrt{5}} f(\alpha + m), m \in \{-1, 1\}\,. \tag{36}$$

Noting that k_{opt} is the smallest of the three vectors, and using Eqs. (34) and (36), we can write the ratio r_s as:

$$r_s = \frac{\tilde{l}^2(\tilde{k}_{opt} + m)}{\tilde{l}^2(\tilde{k}_{opt})} = \left(\frac{f(\alpha + m)}{f(\alpha)}\right)^{-1/2}\,. \tag{37}$$

It can be shown that r_s has a minimum at $\alpha = 0$ irrespective of the value of m. It can also be shown that r_s has two equal-valued maxima at $(\alpha = 0.5, m = 1)$ and at $(\alpha = -0.5, m = -1)$, and thus:

$$\left(\frac{f(1)}{f(0)}\right)^{-1/2} \le r_s \le \left(\frac{f(1.5)}{f(0.5)}\right)^{-1/2} = \left(\frac{f(-1.5)}{f(-0.5)}\right)^{-1/2}\,. \tag{38}$$

Developing Eq. (38) with Eq. (35) yields:

$$\left(\frac{\Phi^2 + \Phi^{-2}}{2}\right)^{-1/2} \le r_s \le \left(\frac{\Phi^3 + \Phi^{-3}}{\Phi + \Phi^{-1}}\right)^{-1/2}\,. \tag{39}$$

Then, using Eq. (12) for the inequality at the left, and Eqs. (9) followed by (8) for the right side, we have:

$$\left(\frac{F_3 + F_1}{2}\right)^{-1/2} \le r_s \le \left(\frac{F_3\sqrt{5}}{\sqrt{5}}\right)^{-1/2}\,, \tag{40}$$

and from Eq. (40) we can easily show that $\sqrt{3/2} < r_s < \sqrt{2}$.

4.5.2 Proof of non-elongation of Voronoi cells

We want to show that the shape of the Voronoi cells of an SFG (characterized by the ratio r_s) remains unchanged when the SFG is scaled using different factors s_x and s_y in each dimension, such that:

$$\begin{cases} x' = s_x\, x \\ y' = s_y\, y \end{cases}\,. \tag{41}$$

Under this scaling transform, the resulting basis vectors $\mathbf{b}'_k$ have the form:

$$\mathbf{b}'_k = \left(\frac{s_x\, F_k}{N}, \frac{s_y\,(-1)^{(k-1)}}{\Phi^k}\right)\,. \tag{42}$$

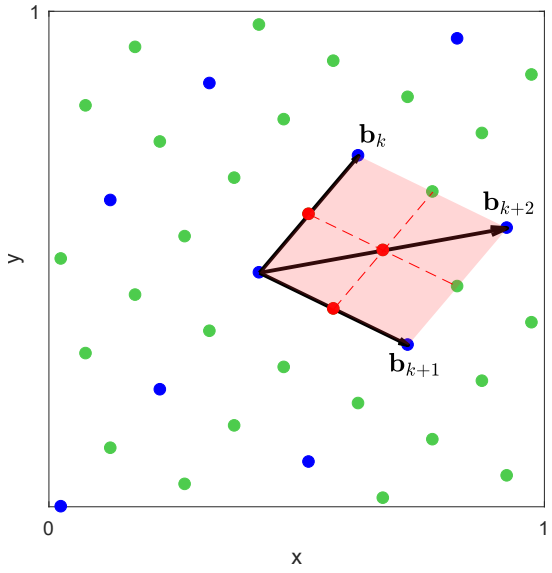

Fig. 6. An extended planar Fibonacci grid. Blue dots show the original grid points. Green and red points show the points resulting from extending the original grid. The pink area corresponds to a unit cell of the original grid formed by the basis vectors $\mathbf{b}_k$ and $\mathbf{b}_{k+1}$. Note how this cell is divided by 4 in the new point set. Note also the red points resulting from halving the basis vectors $\mathbf{b}_k$, $\mathbf{b}_{k+1}$ and $\mathbf{b}_{k+2}$.

By proceeding similarly to the derivation of section 4.4.1, the index k'_{opt} of the smallest basis vector $\mathbf{b}'_k$ is given by:

$$k'_{opt} = \text{nint}\left(\frac{\log(5N^2\Phi^{-4\beta}+1)}{4\log\Phi}\right), \tag{43}$$

with

$$\beta = \frac{\log\left(\frac{s_x}{s_y}\right)}{2\log\Phi}, \quad \text{such that} \quad \frac{s_x}{s_y} = \Phi^{2\beta}. \tag{44}$$

Then, similarly to section 4.4.2 (see Eqs. (28) to (30)), k'_{opt} can be closely approximated by:

$$k'_{opt} \approx \tilde{k}'_{opt} = r - \beta + \alpha' \quad \text{with} \quad -0.5 \leq \alpha' \leq 0.5, \tag{45}$$

and the length $l'^2(k)$ can also be approximated by:

$$l'^2(k) \approx \tilde{l}'^2(k) = s_x\, s_y \left(\frac{\Phi^{2(k+\beta)}}{5N^2} + \Phi^{-2(k+\beta)}\right) \tag{46}$$

Using Eqs. (35), (45) and (46), we can write:

$$\tilde{l}'^2(\tilde{k}'_{opt}) = \frac{s_x\, s_y}{N\sqrt{5}} f(\alpha') \tag{47}$$

and

$$\tilde{l}'^2(\tilde{k}'_{opt} + m) = \frac{s_x\, s_y}{N\sqrt{5}} f(\alpha' + m), \quad m \in \{-1, 1\}. \tag{48}$$

The ratio r'_s is then given by:

$$r'_s = \left(\frac{f(\alpha'+m)}{f(\alpha')}\right)^{-1/2} \quad \text{with} \quad -0.5 \leq \alpha' \leq 0.5, \tag{49}$$

which is equal to r_s, and thus it is also bounded by $\sqrt{3/2} < r'_s < \sqrt{2}$. This shows that the Voronoi cell shape in a planar Fibonacci grid is invariant to stretching transforms.

5 Extensible Spherical Fibonacci Grids

In the following, we propose a new method, called *extensible spherical Fibonacci grids* (E-SFG), for extending spherical Fibonacci grids. In Sec. 5.1, we present our strategy to develop such a method, as well as an algorithm to generate the extended point set. Then, in Sec. 5.2, we present the properties of the extended point set and show that they are in line with those of the original SFG.

Algorithm 1 Extensible Spherical Fibonacci Grid

Inputs:
  $N \leftarrow$ number of points in the initial SF point set
  $L \leftarrow$ number of iteration levels

$F_G \leftarrow \text{fibonacciGrid}(N)$ ▷ Initial point set

$b_0 \leftarrow \text{basisVector}(0, N)$ ▷ Compute the basis vectors
$b_1 \leftarrow \text{basisVector}(1, N)$
$b_2 \leftarrow b_0 + b_1$

for l = 1 to L **do**
  $d \leftarrow 2^l$ ▷ Scaling factor

  $subGrid_0 \leftarrow \text{shiftFibonacciGrid}(F_G, b_0/d)$
  $subGrid_1 \leftarrow \text{shiftFibonacciGrid}(F_G, b_1/d)$
  $subGrid_2 \leftarrow \text{shiftFibonacciGrid}(F_G, b_2/d)$

  $F_G \leftarrow F_G +\!\!+ subGrid_0 +\!\!+ subGrid_1 +\!\!+ subGrid_2$
end for

$\Delta_x \leftarrow (2^{L+1}N)^{-1}$
$finalShift \leftarrow Vector2D(\Delta_x, 0)$
$F_G \leftarrow \text{shiftFibonacciGrid}(F_G, finalShift)$

$ESFG \leftarrow lambertProjection(F_G)$

return $ESFG$

5.1 Approach

Our goal is to develop an algorithm which allows adding more points to an existing SFG, while maintaining the properties of the original distribution. To this end, we proceed by subdividing the unit cell of the planar Fibonacci grid F_G. Let us thus consider the unit cell corresponding to a particular point $\mathbf{p}$ of a planar Fibonacci grid F_G. Such a unit cell is a parallelogram formed by the pair of consecutive basis vectors $(\mathbf{b}_k, \mathbf{b}_{k+1})$ with $\mathbf{p}$ as origin as shown in Fig. 6. Note that, due to the Fibonacci recurrence relation (Eq. (6)), the vertex diagonally opposed to $\mathbf{p}$ is given by $\mathbf{p} + \mathbf{b}_{k+2}$. The unit cell can be easily divided in four equal sub-cells by halving the basis vectors $(\mathbf{b}_k, \mathbf{b}_{k+1})$. Then, three new points can be placed at exactly half-way between $\mathbf{p}$ and $\mathbf{p} + \mathbf{b}_k$, $\mathbf{p} + \mathbf{b}_{k+1}$ and $\mathbf{p} + \mathbf{b}_{k+2}$, respectively, as shown in Fig. 6.

The above strategy provides an effective way of extending the original point set with N points, yielding a new point set with $4N$ points. The final point set can then be seen as the result of adding 3 shifted replications of the original

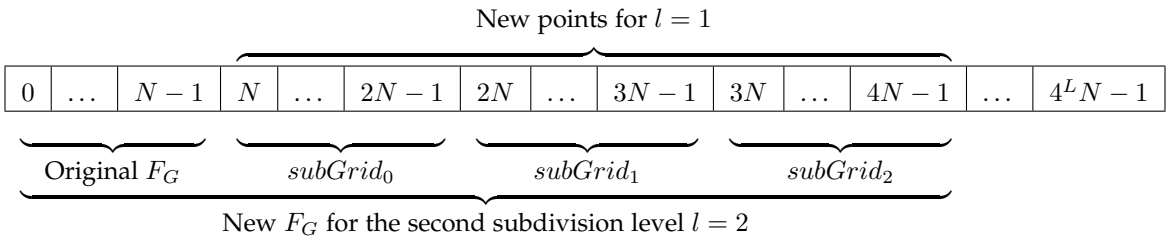

Fig. 7. Representation, as an array of 2D points, of an E-SFG generated using N initial points and L subdivision levels. The numbers in each cell represent the indexes of the points (starting at 0). The first N points correspond to the original F_G grid. The next N points (with indexes N to $2N-1$) correspond to the points generated by shifting the original grid using $\mathbf{b}_0/2$ (line 9 of Alg. 1). The points with index $2N$ to $3N-1$, and $3N$ to $4N-1$ correspond to the points generated by shifting the original grid using $\mathbf{b}_1/2$ and $\mathbf{b}_2/2$, respectively.

point set to get a new extended point set which encompasses the initial point set. However, due to the lack of periodicity of the planar Fibonacci grid along the x-direction, the pair of basis vectors $(\mathbf{b}_k, \mathbf{b}_{k+1})$ must be carefully chosen so as not to exceed the unit square in the non-periodic dimension. As mentioned in Sec. 4.2, such a configuration is obtained with $k = 0$, in which case the basis vectors involved are $\mathbf{b}_0 = (0, -1)$, $\mathbf{b}_1 = (1/N, 1/\Phi)$ and $\mathbf{b}_2 = (1/N, -1/\Phi^2)$. Each (x', y') coordinates of the shifted point set are then simply obtained by:

$$x' = x + x_b/2 \tag{50}$$

$$y' = (y + y_b/2) \bmod 1 \tag{51}$$

where (x, y) are the coordinates of a point $\mathbf{p}$ of the original point set and (x_b, y_b) are the coordinates of any vector of the $\{\mathbf{b}_0, \mathbf{b}_1, \mathbf{b}_2\}$ set. We show in Sec. 5.2 that this simple unit cell subdivision method leads to spherical Fibonacci grids with the same properties as those of the orginal SFG.

Alg. 1 shows the procedure to generate the extensible SFG. The algorithm takes as input arguments the number of points N in the initial point set and the number of iteration levels L. It starts by generating an initial planar Fibonacci grid F_G with N points using the classic algorithm. This grid is then extended in the planar domain by repeating L times the process mentioned above, thus multiplying by 4 the point set size at each iteration. The E-SFG is finally produced by projecting the extended planar grid from the unit square to the unit sphere through the Lambert cylindrical projection. In this way, the $4^L N$ points of the resulting E-SFG contain the N points of the initial SFG.

In line 3 of Alg. 1 an initial planar Fibonacci grid with N points is generated and stored in F_G. In lines 4 to 6, the basis vectors $\mathbf{b}_0$, $\mathbf{b}_1$ and $\mathbf{b}_2$ are computed. Then, a loop with as many cycles as the number of subdivision levels L starts (line 7). At each iteration, the scalar d used to scale down the basis vectors is updated. This instruction is followed by three separate calls to the function shiftFibonacciGrid(), with different arguments (lines 9 to 11). This function, receives an initial grid (in this case through the variable named F_G), and a vector indicating the direction and magnitude of a shifting operation to apply to the initial grid. The shifted grid is then returned as result. This operation is repeated for the three used basis vectors. Note that the size of the basis vector depends on the extension level considered. The planar F_G is updated in line 12 by concatenating the original points with the new points resulting in the extended planar Fibonacci grid (where $+\!\!+$ is the concatenation operator). Once the grid has been extended L times, it is shifted (lines 14 to 16). Similarly to Swinbank et al. [28], we apply a final shift Δ_x to the x-coordinates of the planar grid, which further reduces the spherical discrepancy by symmetrizing the distribution of the points with respect to the poles. The value of the shift is $\Delta_x = \left(2^{L+1}N\right)^{-1}$, i.e., a value equal to $(x_{max} - 1/2)$, where x_{max} is the distance between the grid point with the larger x-coordinate and the unit square edge $x = 1$. Note that this shift is not optimal for the lower levels $l < L$, since these levels are not symmetrically shifted using Δ_x. However, this non-optimality has no discernible impact in the final results as we show later. Finally, the extended planar Fibonacci grid is projected onto the sphere in line 17. An example of an E-SFG with $N = 64$ generated with initial points and $L = 2$ subdivision levels is shown in Fig. 1. A general schematic representation of the final E-SFG generated by Alg. 1 is shown in Fig. 7. In practice, the E-SFG is intended to be used as follows: (i) first pre-compute the complete E-SFG with L subdivision levels; (ii) during rendering, the rendering application progressively extracts the new points corresponding to the current desired sampling level l from the pre-computed sequence.

5.2 Properties of E-SFGs

As shown in Fig. 1, the new points generated by E-SFG look seamlessly embedded in the original point set thanks to the unit cell subdivision strategy described in Sec. 5.1. Moreover, as shown in the following, the properties of SFGs described in Sec. 4 are preserved. Let us start by analyzing the minimum distance between samples. Since the length of the basis vectors of the E-SFG is equal to that of the basis vectors of the original planar F_G up to a factor of $1/2^l$, Eq. (24) still holds. Therefore, the minimum distance between neighboring points d_{min} stays in the same bounds as for an SFG set of the same size. Furthermore, the non-elongation property of the Voronoi cells is also preserved since their shape is left unchanged in the subdivision process. However, note that for equal point set sizes, E-SFGs and SFGs have Voronoi cells which are always different. Indeed, the basis vectors of SFGs change both in size and direction with the point set size, whereas their direction remains unchanged for E-SFGs spawned from the same SFG initial set. Finally, it is straightforward to see that SFG and E-SFG point sets of the same size have the same unit cell area. Consequently, the important geometric properties of planar

Fibonacci grids are preserved in the extended grids and, by examining Fig 1, we can see the great similarity between the resulting SFG and E-SFG point distributions.

5.3 Progressivity

At each iteration level, the point set size is multiplied by 4, as opposed to the $\times 2$ increasing rate of the typical $(0,2)$-sequences utilized in computer graphics. This could be considered a drawback due to a lack of progressivity. However, recall that the rate of decrease of integration error seldom exceeds $\mathcal{O}(N^{-0.75})$ in rendering (cf. [19]), which means that a $\times 4$ set size increase entails an error decrease in a reasonable $4^{-0.75} = 2.8$ ratio at best. Moreover, the practical application to adaptive rendering shown later in Fig. 12 confirms that this feature does not hinder adaptive sampling. Such an approach is thus appropriate for rendering applications.

For applications requiring more progressivity, Alg. 1 can be slightly modified to ensure a $\times 2$ progressivity with interesting properties. The basic idea is to use a single shifted replication of the current point set using a translation vector $\mathbf{b}_s/2$ chosen among $\mathbf{b}_0/2$, $\mathbf{b}_1/2$, $\mathbf{b}_2/2$, so as to create an intermediate point set with of double size. Then, the following step will use the remaining two translation vectors to retrieve the original $\times 4$ refinement step. As a result, the shifted point set is one among $subGrid_0$, $subGrid_1$ or $subGrid_2$, depending on the chosen $\mathbf{b}_s$, and it can be reused afterwards in the $\times 4$ step. To keep the uniformity of the duplicated point distribution as good as possible, $\mathbf{b}_s$ is chosen so as to keep the shape of the Voronoi cell as compact as possible. Considering the Voronoi cell shown in Fig. 4(a), this best translation vector is logically $\mathbf{b}_g/2$ where $\mathbf{b}_g$ is the longest vector among the three vectors that define the Voronoi cell. However recall that the periodicity property of the planar Fibonacci grids F_G imposes a choice of translation vector among $\mathbf{b}_0/2$, $\mathbf{b}_1/2$ and $\mathbf{b}_2/2$, and the best translation vector $\mathbf{b}_g$ does not fulfill this requirement in general. This problem is easily solved because, as shown below, a shifted replication with a $\mathbf{b}_g/2$ translation vector is equally obtained with a vector $\mathbf{b}_s/2$ such that $s = g \bmod 3$.

In what follows, we provide a proof of $s = g \bmod 3$. Let us first observe that a Fibonacci number F_k is even if $k \bmod 3 = 0$ and odd otherwise. We start by showing that any basis vectors $\mathbf{b}_k$ can be expressed as a linear combination of $\mathbf{b}_0$ and $\mathbf{b}_1$. To this end, we rewrite the basis vector equation given by Eq. (5) as:

$$\mathbf{b}_k = F_k \left(\frac{1}{N}, \frac{1}{\Phi} \right) - \left(0, \frac{F_k}{\Phi} \right) + \left(0, \frac{(-1)^{k-1}}{\Phi^k} \right) . \quad (52)$$

From Eq. (5), we have that $\mathbf{b}_0 = (0,-1)$ and $\mathbf{b}_1 = (N^{-1}, \Phi^{-1})$. Then, using Eq. (10), Eq. (52) can be re-written as:

$$\mathbf{b}_k = F_k \, \mathbf{b}_1 + F_{k-1} \, \mathbf{b}_0 , \quad (53)$$

which completes the first step of the proof. Using Eq. (53), we can now write $\mathbf{b}_g/2$ as:

$$\frac{\mathbf{b}_g}{2} = \frac{F_{g-1} \, \mathbf{b}_0}{2} + \frac{F_g \, \mathbf{b}_1}{2} . \quad (54)$$

Eq. (54) shows the shift of the lattice along $\mathbf{b}_g/2$ as a composition of two independent translations. When F_{g-1} is even, then F_g is surely odd, and the coefficient $F_{g-1}/2$ of $\mathbf{b}_0$ is an integer. Consequently, the translation along $(F_{g-1} \, \mathbf{b}_0)/2$ yields exactly the same lattice. In this case, the generation of new points by shifting the lattice along $\mathbf{b}_g/2$ is thus due to the translation by $F_g \, (\mathbf{b}_1/2)$. As F_g is an integer, the translation by $F_g \, (\mathbf{b}_1/2)$ amounts to a translation along $\mathbf{b}_1/2$. A similar argument can be made when F_g is even: in this case, F_{g-1} is surely odd, and shifting the lattice along $\mathbf{b}_g/2$ can thus be reduced to a translation along $\mathbf{b}_0/2$. When both F_g and F_{g-1} are odd, then we have $F_g = 2m+1$ and $F_{g-1} = 2n+1$, and Eq. (54) can be rewritten as:

$$\frac{\mathbf{b}_g}{2} = n \, \mathbf{b}_0 + m \, \mathbf{b}_1 + \frac{\mathbf{b}_2}{2} . \quad (55)$$

In this case, since both m and n are integers, shifting the lattice along $\mathbf{b}_g/2$ amounts to a translation by $\mathbf{b}_2/2$.

Given that the parity of the Fibonacci numbers follows a ternary cycle (even-odd-odd, even-odd-odd, ...), the index s is simply given by:

$$s = g \bmod 3 . \quad (56)$$

Since s is the index of the larger basis vector among $\mathbf{b}_{k_{opt}-1}$ and $b_{k_{opt}+1}$, and since k_{opt} only depends on N (i.e., the original point set size, c.f. Eq. (23)), s can be easily computed at the beginning of Alg. 1. Indeed, once k_{opt} is known, Eq. (5) can be used to calculate $\mathbf{b}_{k_{opt}-1}$ and $\mathbf{b}_{k_{opt}+1}$, compute their norm, and hence determine s. Then, by replacing the concatenation in line 12 of Alg. 1 by a reordered concatenation, we ensure that the $subGrid$ resulting from the shift using $\mathbf{b}_s/2$ is the first in the concatenation. This allows for a smoother progressivity of the E-SFG point set. To this end, line 12 of Alg. 1 is thus replaced by:

```
1: if s = 0 then
2:     F_G ← F_G + subGrid_0 + subGrid_1 + subGrid_2
3: else if s = 1 then
4:     F_G ← F_G + subGrid_1 + subGrid_2 + subGrid_0
5: else if s = 2 then
6:     F_G ← F_G + subGrid_2 + subGrid_0 + subGrid_1
7: end if
```

At each iteration level l, the resulting point set F_G is thus a concatenation of the initial point set F_G, at the current iteration level, with the three new shifted point sets $subGrid_0$, $subGrid_1$ and $subGrid_2$. Recall that these new shifted point sets are computed by applying the basis vectors $\mathbf{b}_0/d$, $\mathbf{b}_1/d$ and $\mathbf{b}_2/d$, respectively, with $d = 2^l$ as in line 9 of Alg. 1. To allow for a $\times 2$ progressivity, the order of the concatenation is chosen such that the first subset among $subGrid_0$, $subGrid_1$ and $subGrid_2$ concatenated with F_G is the one computed using the basis vector $\mathbf{b}_s$. Henceforth we will refer to this chosen subset as $subGrid_s$. During rendering, the application can simply take the first new set of points (i.e., $subGrid_s$) at each iteration level in order to double the number of points used for sampling. An example of this intermediate subdivision step, corresponding to the $\times 2$ subdivision between Fig. 1(a) and (b), is shown in Fig. 8. To double again the number of points, the other two remaining sub-grids should be used. This process is repeated for each iteration level until the maximum number of levels (L is Alg. 1) is reached.

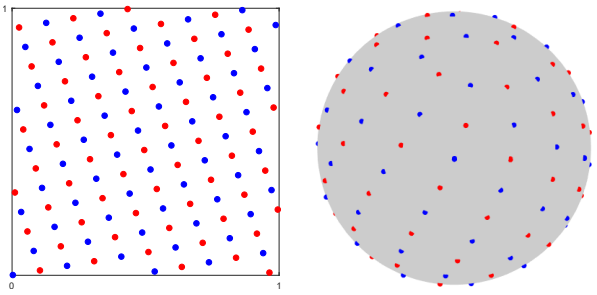

Fig. 8. Intermediate $\times 2$ subdivision step between 64 and 256 points corresponding to Fig.1(a) and (b), respectively. The resulting point set contains 128 points. The blue dots represent the points in the initial grid. The red dots represent the new points obtained by shifting the initial grid using the basis vector $\mathbf{b}_s$ (where s is given by Eq. (56)). Left: planar grid. Right: after spherical projection. Note that the point distribution is slightly less uniform than than in the $\times 4$ point set c.f. Fig. 1.

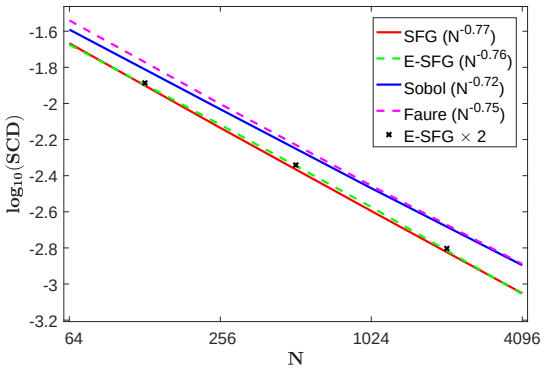

Fig. 9. Spherical cap discrepancy (SCD) as a function of the number of samples, on a logarithmic scale. The figure shows the SCD and its convergence rate (in-between parenthesis) for an E-SFG (green line), the original spherical Fibonacci grid (SFG, red), and the Sobol and the Faure sequences projected onto the sphere with the Lambert cylindrical projection (in blue and magenta, respectively). The tested point set sizes correspond to a 3-level E-SFG applied to an initial 64-point SFG set, yielding 64, 256, 1024 and 4096 points. The black 'x' markers show the SCD of E-SFG point sets generated through the intermediate $\times 2$ subdivision method proposed in Sec. 5.3.

6 Results

In this section, we assess the quality of E-SFG point sets. First we evaluate the E-SFG by resorting to a spherical metric of the point set uniformity, i.e., the spherical cap discrepancy (Sec. 6.1). Then, we evaluate the performance of the E-SFG in rendering application cases (i.e., Quasi-Monte Carlo estimates of the illumination integral in Sec. 6.2). In both evaluations, the obtained E-SFGs are compared to the original SFG (not extensible), and to two familiar hierarchical low discrepancy sequences: the Sobol sequence [25], and the Faure sequence [11].

6.1 Spherical Cap Discrepancy of E-SFGs

To assess the quality of the proposed E-SFG, we have evaluated the resulting point sets using the spherical cap discrepancy (SCD) [5], [19], [26], [27]. Informally speaking, the SCD can be thought of as the unit sphere equivalent of the unit square star discrepancy [20]. It characterizes the equidistribution of a spherical point set [15], and measures the efficiency of a point set for QMC integration over the sphere. Smaller SCD values imply a more uniform point set distribution and result in a smaller QMC estimation error. Ideally, for any spherical cap, the ratio between the point set size and the number of points lying in the spherical cap should be equal to the proportion between the area of the sphere and the area of the spherical cap. The SCD measures the average difference between the two ratios. Thanks to Stolarsky's invariance principle [26], [27], the SCD of a spherical point set can be related to the sum of distances between the samples, yielding a simple closed-form analytic expression. Given a spherical point set P_N with N points, its SCD is given by [5], [19]:

$$\mathrm{SCD}(P_N) := \frac{1}{\sqrt{2}} \left(\frac{4}{3} - \frac{1}{N^2} \sum_{j=1}^{N} \sum_{i=1}^{N} \|p_i - p_j\| \right)^{1/2}, \quad (57)$$

where the p_k are sample points on the sphere, and the operator $\|p_i - p_j\|$ denotes the euclidean distance between the points p_i and p_j.

Fig. 9 shows the value of the SCD as a function of the number of samples on a logarithmic scale for the basic SFG, our proposed E-SFG, a Sobol sequence and a Faure sequence projected onto the sphere. The results show that the original SFG and the E-SFG exhibit a very similar SCD, independent of the point set size considered. Moreover, the SCD rate of decrease with N approaches the optimal rate of spherical low-discrepancy sequences $\mathcal{O}(N^{-0.75})$ [1] for both methods. As regards the comparison with existing hierarchical sampling methods, we can observe that E-SFG achieves significantly better results than point sets produced with Sobol or Faure sequences. Indeed, the discrepancy of E-SFG is consistently less than that of the Sobol and Faure sequences, and the rate of decrease of the E-SFG is also slightly better. Finally, note that the SCD of the point sets obtained with the intermediate subdivision step, as suggested in Sec. 5.3, is in line with the SCD of the $\times 4$ E-SFGs point sets proposed in Sec. 5.1, which validates our $\times 2$ progressivity solution.

6.2 A Practical Application to Rendering

The application of the E-SFG point sets to rendering is straightforward. We follow a similar approach to that of Marques et al. [19], where an original hemispherical point set is warped taking into account the BRDF shape. This approach is the Quasi-Monte Carlo equivalent to the *importance sampling* technique broadly used in stochastic Monte Carlo. In the following we present two test cases. The first one, illustrated through the Happy Buddha scene (Figs. 10 and 11), shows that E-SFGs have similar performance to that of the original (non-extensible) SFG point sets, and outperform the other considered point sets, whatever the sampling level considered. The second test case, illustrated through the Cornell Box scene (Fig. 12), shows that the E-SFG can be efficiently applied to a real adaptive sampling rendering case.

Fig. 10 shows a set of rendering results for the *Happy Buddha* scene. The material of the Happy Buddha is modeled through a modified Phong BRDF with a shininess exponent of 20. To reduce the rendering time and without loss of generality, the incident light is given by an environment

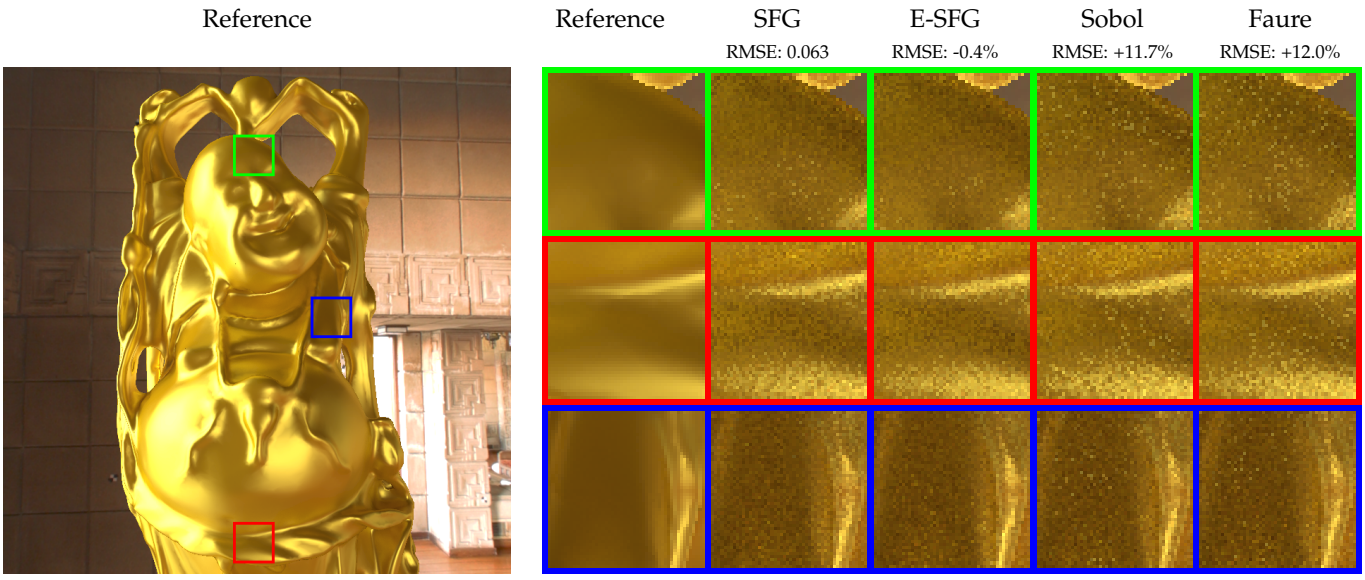

Fig. 10. Rendering results for the *Happy Buddha* scene. The used BRDF is a modified Phong BRDF with a shininess exponent of 20. The close-up views show a comparison between an image rendered using the original spherical Fibonacci point sets, our E-SFG point set, a Sobol sequence and a Faure sequence. The used E-SFG was generated using 2 iteration levels and an initial number of points $N = 8$, resulting in a 128-point set. During rendering, to sample the glossy component, the first 32 samples resulting from the first iteration level of the E-SFG have been used. To sample the diffuse component, the full E-SFG with 128 points has been used. The displayed RMSE figures of the images generated with E-SFG, Sobol and Faure are computed relatively to that of the image generated with SFG.

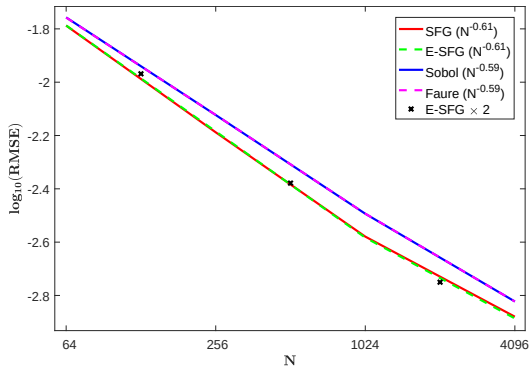

(a) Diffuse

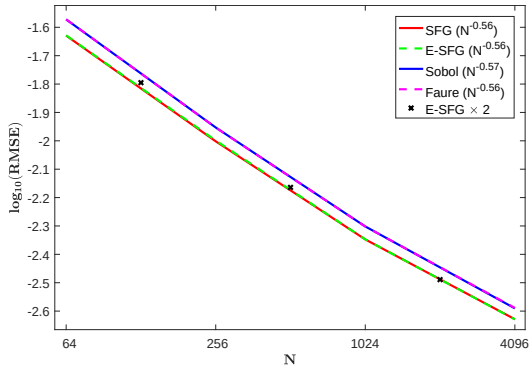

(b) Glossy 20

Fig. 11. RMSE for the *Happy Buddha* scene, considering a pure diffuse BRDF (a) and a pure glossy modified Phong BRDF with shininess exponent 20. The black 'x' markers show the RMSE of E-SFG point sets generated through the intermediate $\times 2$ subdivision method proposed in Sec. 5.3. The convergence rate for each method is given in the legend, in-between parenthesis.

map. The results show that the performance of the original SFG and that of our proposed E-SFG are similar, and also that both methods outperform the tested low discrepancy sequences (Sobol and Faure). Indeed, the close-up views show that the noise is clearly lower for the E-SFG and SFG. This observation is confirmed by the root mean squared error (RMSE) analysis. The image generated with E-SFG has a roughly similar RMSE to that of the SFG-based image (-0.4%), while the images generated with Sobol and Faure point sets exhibit a RMSE that is 11.7% and 12.0% larger than that of the SFG, respectively.

Fig. 11 depicts the RMSE as a function of the number of samples for the *Happy Buddha* scene, considering a pure diffuse and a pure glossy Phong BRDF (with shininess factor 20). The results show that, for the same number of samples, and for any point set size, an E-SFG has a similar performance to that of an SFG, and consistently outperforms the Sobol and Faure low discrepancy sequences projected onto the sphere using the Lambert cylindrical transform. Moreover, the intermediate subdivision step (noted by E-SFG $\times 2$) yields RMSE values which are approximately in line with the RMSE values obtained for the $\times 4$ E-SFG. These results confirm the SCD results of Fig. 9.

Finally, Fig. 12 shows a set of results for the Cornell Box scene. This scene has BRDFs with different shininess values, and the incident illumination is computed by the gathering step of photon mapping. The rendered images have been generated using a single ray per pixel traced from the viewpoint. This ray intersects the scene at a point (*shading point*) for which the illumination integral is estimated. The number of samples is chosen adaptively, during rendering, according to three sampling levels. The number of samples per sampling level is one among $[20, 80, 320]$ and $[40, 160, 640]$ for the glossy and diffuse components, respectivelly. The sampling level is selected by evaluating

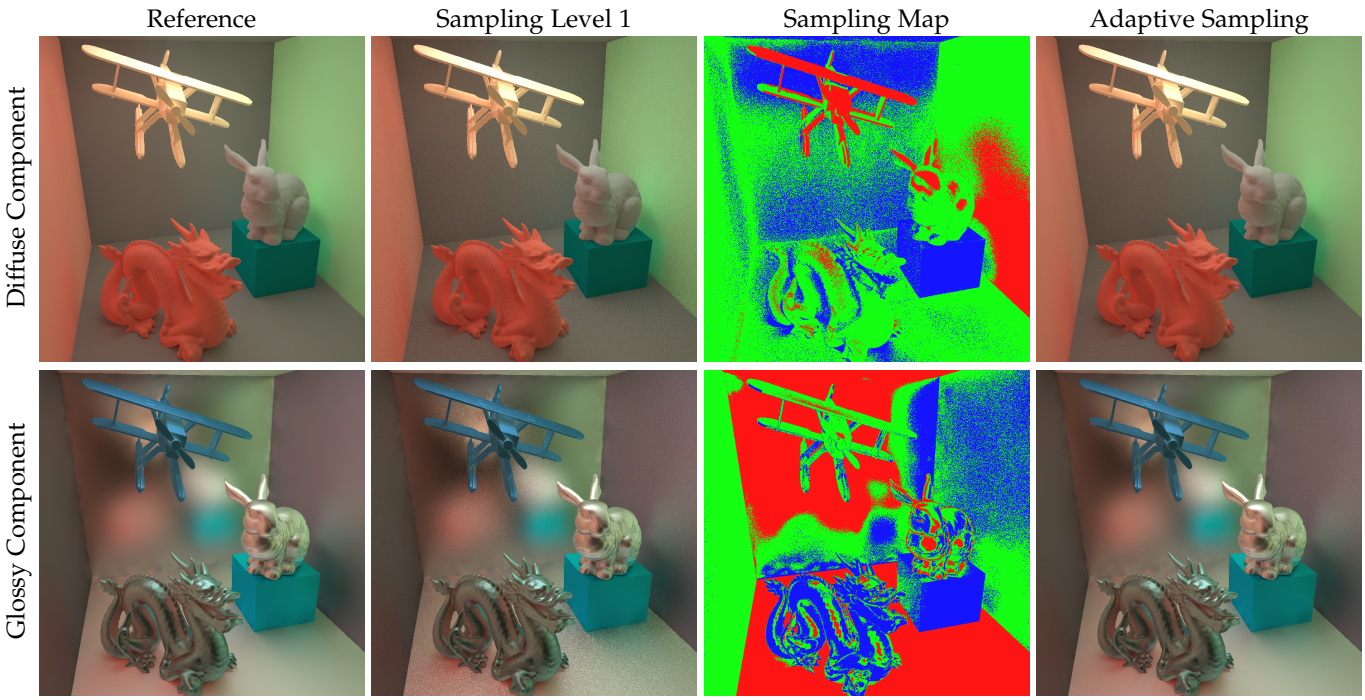

Fig. 12. Rendering results for the *Cornell Box* scene using our extended spherical Fibonacci grid (E-SFG) in an adaptive sampling setting, where the number of samples is adaptively chosen for each shading point. The number of samples per sampling level is of $[20, 80, 320]$ and $[40, 160, 640]$ for the glossy and diffuse components, respectively. The three sampling levels are represented in blue (level-1), green (level-2) and red (level-3) in the respective sampling map. The resulting number of pixels per level for the diffuse case is: 128580 for level-1, 326726 for level-2 and 63094 for level-3. For the glossy case we have: 130863 for level-1, 206817 for level-2 and 180720 for level-3. The total number of used samples for the adaptive sampling-based image is thus 9.78×10^7 for the diffuse case and 7.70×10^7 for the glossy case.

the samples' color entropy [22] at the current sampling level. If the entropy is above a user given threshold, then we move on to the next sampling level. The results show that a reasonable number of pixels is selected at each sampling level. Moreover, the final adaptive sampling-based image is of comparable quality to the reference image, and it clearly improves over the basic level-1 sampling image, while bringing a significant saving in computing cost compared with a uniform point set size solution (due to the reduction in the number of used samples). This shows that the ESFG is well-suited to adaptive rendering.

7 Discussion

In the following, we discuss specific limitations of our proposed E-SFGs. Generally speaking, E-SFGs should not be seen as a substitute to SFGs. Indeed, as discussed below, the constraint of maintaining the previous points from one iteration to another has side effects at the poles when l is large as discussed below. Instead, E-SFGs should be regarded as solution which enables adaptive sampling in typical rendering settings, where a number of samples ranging from N to $4^3N = 64N$, that is three $\times 4$ sampling levels (or 6 levels if the $\times 2$ progressivity is implemented), is sufficient. In this context, E-SFGs provide a similar rendering quality to that obtained with SFGs, hence clearly outperforming alternative hierarchical point sets such as Sobol and Faure.

Finite sequence: The proposed E-SFG algorithm generates a finite number of points, as opposed to the low discrepancy sequences which are able to generate infinite sequences of points and thus do not require the maximum number of points to be known beforehand. In our opinion, this is not too constraining, since in most CG applications a maximum number of points can be assumed without compromising the final result.

Distribution around the poles: At each subdivision level l, the E-SFG doubles the number of points with the same polar angle θ, yielding 2^l points sharing the same polar angle. These 2^l points are thus aligned on a circle at a close distance to the pole, which is not the case of the original SFG for which each point has a different polar angle. This is not a problem in practice as the concerned subset size (2^l) is small compared to the whole set size (e.g. $2^3 = 8$ compared to 1280 for a 3-level E-SFG starting at 20 points). Moreover, it can be seen from Figs. 9 and 11 that both the spherical cap discrepancy and the root mean squared error of E-SFG point sets are almost identical to the one of SFG sets of the same size, which confirms our analysis.

8 Conclusions

In this article we have proposed a method that generates extensible spherical Fibonacci grids (E-SFG). We have based our point set extension strategy on an in-depth analysis of the properties of classic SFGs, which demonstrates why classic SFGs generate highly uniform *spherical* distributions of points. Thanks to a point set extension algorithm which preserves such properties, our experiments showed that the performance of our proposed E-SFGs is very close to those of SFGs of the same size. Furthermore, we have shown that the same $\times 2$ progressivity rate as the one achieved by familiar low-discrepancy sequences can be obtained with

E-SFGs. We have successfully reached the goal of extending an original point set without impairing its properties. Moreover, we have also shown that an E-SFG performs better than familiar extensible low discrepancy sequences projected onto the sphere. In particular, our rendering experiments have shown that E-SFG point sets perform as well as SFG and significantly better than Sobol and Faure sequences. Finally, we have shown that E-SFGs are well-suited to adaptive sampling and provide significant savings in computing load when applied to rendering problems.

ACKNOWLEDGMENTS

Ricardo Marques was supported by the European Union's Horizon 2020 research programme through a Marie Sklodowska-Curie Individual Fellowship (grant number 707027).

REFERENCES

[1] C. Aistleitner, J.S. Brauchart, and J. Dick. Point Sets on the Sphere $\mathbb{S}^2$ with Small Spherical Cap Discrepancy. *Discrete & Computational Geometry*, pages 1–35, 2012.

[2] N. Antonello, E. De Sena, M. Moonen, P. A. Naylor, and T. van Waterschoot. Room impulse response interpolation using a sparse spatio-temporal representation of the sound field. *IEEE/ACM Transactions on Audio, Speech, and Language Processing*, 25(10):1929–1941, Oct 2017.

[3] James Arvo. Stratified sampling of spherical triangles. In *Proceedings of the 22Nd Annual Conference on Computer Graphics and Interactive Techniques*, SIGGRAPH '95, pages 437–438, New York, NY, USA, 1995. ACM.

[4] Andrea Baldacci, Rastislav Kamenický, Adam Riečický, Paolo Cignoni, Roman Ďurikovič, Roberto Scopigno, and Martin Madaras. Gpu-based approaches for shape diameter function computation and its applications focused on skeleton extraction. *Computers & Graphics*, 59(Supplement C):151 – 159, 2016.

[5] Johann S. Brauchart and Josef Dick. Quasi-monte carlo rules for numerical integration over the unit sphere $\mathbb{S}^2$. *Numer. Math.*, 121(3):473–502, 2012.

[6] J. Cassels. *An Introduction to the Geometry of Numbers*. Springer-Verlag Berlin Heidelberg, 1997.

[7] Ronald Cools and Dirk Nuyens. Extensions of fibonacci lattice rules. In Pierre L' Ecuyer and Art B. Owen, editors, *Monte Carlo and Quasi-Monte Carlo Methods 2008*, pages 259–270, Berlin, Heidelberg, 2009. Springer Berlin Heidelberg.

[8] Sabrina Dammertz and Alexander Keller. Image synthesis by rank-1 lattices. In Alexander Keller, Stefan Heinrich, and Harald Niederreiter, editors, *Monte Carlo and Quasi-Monte Carlo Methods 2006*, pages 217–236, Berlin, Heidelberg, 2008. Springer Berlin Heidelberg.

[9] Sabrnina Dammertz, Holger Dammertz, and Alexander Keller. Efficient search for low-dimensional rank-1 lattices with applications in graphics. In *Proc. Monte Carlo and Quasi-Monte Carlo Methods 2008*, pages 271–287. Springer, 2008.

[10] Alun Evans, Javi Agenjo, and Josep Blat. A pipeline for the creation of progressively rendered web 3d scenes. *Multimedia Tools and Applications*, (to appear):1–29, Dec 2017.

[11] Henri Faure. Discrépance de suites associées à un système de numération (en dimension s). *Acta Arithmetica*, 41(4):337–351, 1982.

[12] Álvaro González. Measurement of Areas on a Sphere Using Fibonacci and Latitude–Longitude Lattices. *Mathematical Geosciences*, 42:49–64, 2010.

[13] Ronald L. Graham, Donald E. Knuth, and Oren Patashnik. *Concrete Mathematics: A Foundation for Computer Science*. Addison-Wesley Longman Publishing Co., Inc., Boston, MA, USA, 2nd edition, 1994.

[14] J H Hannay and J F Nye. Fibonacci Numerical Integration on a Sphere. *Journal of Physics A: Mathematical and General*, 37(48):11591, 2004.

[15] DP Hardin, T Michaels, and EB Saff. A comparison of popular point configurations on $\mathbb{S}^2$. *Dolomites Research Notes on Approximation*, 9(1):16–49, 2016.

[16] Fred J. Hickernell, Hee Sun Hong, Pierre L'Ecuyer, and Christiane Lemieux. Extensible lattice sequences for quasi-monte carlo quadrature. *SIAM J. Sci. Comput.*, 22(3):1117–1138, March 2000.

[17] Benjamin Keinert, Matthias Innmann, Michael Sänger, and Marc Stamminger. Spherical fibonacci mapping. *ACM Trans. Graph.*, 34(6):193:1–193:7, October 2015.

[18] Alexander Keller. Stratification by rank-1 lattices. In Harald Niederreiter, editor, *Monte Carlo and Quasi-Monte Carlo Methods 2002*, pages 299–313, Berlin, Heidelberg, 2004. Springer Berlin Heidelberg.

[19] R. Marques, C. Bouville, M. Ribardière, L. P. Santos, and K. Bouatouch. Spherical Fibonacci Point Sets for Illumination Integrals. *Computer Graphics Forum*, 32(8):134–143, December 2013.

[20] H. Niederreiter. *Random Number Generation and Quasi-Monte Carlo Methods*. CBMS-NSF Regional Conference Series in Applied Mathematics. Society for Industrial and Applied Mathematics, 1992.

[21] Harald Niederreiter and Ian H. Sloan. Integration of nonperiodic functions of two variables by Fibonacci lattice rules. *Journal of Computational and Applied Mathematics*, 51(1):57 – 70, 1994.

[22] Jaume Rigau, Miquel Feixas, and Mateu Sbert. Entropy-based adaptive sampling. In *Graphics Interface*, 2003.

[23] I. H. Sloan and S. Joe. *Lattice methods for multiple integration / I.H. Sloan and S. Joe*. Clarendon Press ; Oxford University Press Oxford : New York, 1994.

[24] Ian H. Sloan. Lattice methods for multiple integration. *Journal of Computational and Applied Mathematics*, 12-13(Supplement C):131 – 143, 1985.

[25] I.M. Sobol. On the Distribution of Points in a Cube and the Approximate Evaluation of Integrals. *USSR Computational Math. and Math. Phys.*, 7:86–112, 1967.

[26] Kenneth B. Stolarsky. Sums of distances between points on a sphere. II. *Proc. of the AMS*, (2), December 1973.

[27] Kenneth B. Stolarsky. Discrepancy and sums of distances between points of a metric space. In L. M. Kelly, editor, *The Geometry of Metric and Linear Spaces*, pages 44–56, Berlin, Heidelberg, 1975. Springer Berlin Heidelberg.

[28] Richard Swinbank and R. J. Purser. Fibonacci grids: A novel approach to global modelling. *Quarterly Journal of the Royal Meteorological Society*, 132(619):1769–1793, 2006.

[29] Jianing Zhang. On numerical orientation averaging with spherical fibonacci point sets and compressive scheme. *Journal of Quantitative Spectroscopy and Radiative Transfer*, 206(Supplement C):1 – 7, 2018.

Ricardo Marques Ricardo Marques is Lecturer at the Universitat Pompeu Fabra (UPF), Barcelona. He received his MSc degree from University of Minho, Portugal (2009), after which he worked as a researcher in the same university. He joined INRIA (Institut National de Recherche en Informatique et Automatique) and the FRVSense team as a PhD student in the fall 2010 under the supervision of Kadi Bouatouch. In his thesis, he focused on spherical integration methods applied to light transport simulation. He defended his PhD thesis in the fall 2013 and joined the Mimetic INRIA research team as a research engineer in 2014, where he worked in the field of Crowd Simulation. From summer 2016 to summer 2018 he worked in the Interactive Technologies Group (GTI) of UPF as a post-doc, supported by a Marie Sklodowska-Curie individual fellowship.

Christian Bouville Christian Bouville is presently invited researcher in the Percept team at IRISA (Institut de Recherche en Informatique et Systémes Aléatoires) in Rennes (France). He has been team leader, project leader and Emeritus expert at Orange Labs until 2006 and has been involved in many European and national projects. His main fields of research are now global illumination models and image perception with a special interest in machine learning approaches.

Kadi Bouatouch was an electronics and automatic systems engineer (ENSEM 1974). He was awarded a PhD in 1977 and a higher doctorate in computer science in the field of computer graphics in 1989. He is working on global illumination, lighting simulation for complex environments, GPU based rendering and computer vision. He is currently Emeritus Professor at the University of Rennes 1 (France) and researcher at IRISA (Institut de Recherche en Informatique et Systémes Aléatoires). He is member of Eurographics.

Josep Blat Josep Blat received his Ph.D. degree in mathematics from Heriot-Watt University, Edinburgh, U.K., in 1985. He is currently a Full Professor in the Department of Information and Communication Technologies at Universitat Pompeu Fabra, Barcelona, Spain, where he leads a research group in Interactive Technologies. After his initial research in Applied Nonlinear Analysis, he moved to modeling and mathematical analysis of images (collective prize Philip Morris France 1991). His current research interests include 3-D graphics (web-based expressive human animation, games, rendering), and humancomputer interaction (older people, children, ethnography, geolocation, wearables and haptics).